



LNF-00/030 (IR)
14 Novembre 2000

PERFORMANCES OF THE FINUDA DRIFT CHAMBERS IN A COSMIC RAY TEST

M. Agnello¹, M. Bertani², E. Botta³, D. Calvo³, P. Cerello³, F. De Mori⁴,
G. D'Erasmus⁵, A. Feliciello³, A. Filippi³, V. Filippini⁶, P. Gianotti², G. Gómez⁷,
S. Marcello³, O. Morra⁸, A. Panzarasa⁹, G. Tagliente⁵, L. Venturelli⁷

1) *Dip. di Fisica del Politecnico di Torino, C.so Duca degli Abruzzi 24, I-10129 Torino, Italy;*
INFN, Sez. di Torino, Via Giuria 1, I-10125 Torino, Italy;

2) *INFN, Laboratori Nazionali di Frascati, Via Fermi 40, I-00044 Frascati, Italy;*

3) *INFN, Sez. di Torino, Via Giuria 1, I-10125 Torino, Italy;*

4) *Dip. di Fisica, Università di Trieste, Via Valerio 2, I-34127 Trieste, Italy; INFN,*
Sez. di Trieste, Via Valerio 2, I-34127 Trieste, Italy;

5) *INFN, Sez. di Bari, Via Amendola 173, I-70126 Bari, Italy; Dip. di Fisica,*
Università di Bari, Via Amendola 173, I-70126 Bari, Italy;

6) *INFN, Sez. di Pavia, Via Bassi 6, I-27100 Pavia, Italy;*

7) *Dip. di Chimica e Fisica per l'Ingegneria e per i Materiali, Università di Brescia,*
Via Valotti 9, I-25133 Brescia, Italy;
INFN, Sez. di Pavia, Via Bassi 6, I-27100 Pavia, Italy;

8) *CNR, Istituto di Cosmogeofisica, C.so Fiume 4, I-10131 Torino, Italy;*
INFN, Sez. di Torino, Via Giuria 1, I-10125 Torino, Italy;

9) *Dip. di Fisica Sperimentale, Università di Torino, Via Giuria 1, I-10125 Torino, Italy;*
INFN, Sez. di Torino, Via Giuria 1, I-10125 Torino, Italy;

Abstract

We report on a cosmic ray test of the FINUDA drift chambers performed inside the FINUDA detector without a magnetic field. From an accurate study of the drift cell space-time relations we determine both the spatial resolution and the mechanical alignment of the chambers. The chambers operate with a non-saturated 70% He - 30% iC₄ H₁₀ gas mixture and the drift cells are modeled using GARFIELD. After alignment of the drift chamber system, we find a spatial resolution averaged over the entire drift cell and over all angles of incidence of about 140 μm.

1 Introduction

The FINUDA experiment [1,2] at the DAΦNE e^+e^- ϕ -factory is devoted to the study of the formation of Λ -hypernuclei from the reaction $K_{\text{stop}}^- + {}^A Z \rightarrow {}^A_\Lambda Z + \pi^-$ on nuclear targets and of their subsequent decay. Low energy (~ 16 MeV) K^- from the ϕ decay are stopped in very thin ($0.3 - 0.5$ g/cm²) targets, allowing unprecedented production rate and energy resolution on the hypernuclear levels. The energy of the prompt π^- emitted following hypernucleus formation is directly related to the energy levels of the hypernucleus.

FINUDA is a high-resolution magnetic spectrometer arranged following a cylindrical geometry around the DAΦNE beam pipe. It consists of a superconducting solenoid which provides a uniform magnetic field of 1.1 T, Si μ -strip detectors, two layers of low mass drift chambers (LMDC) and six layers of straw-tubes in a stereo assembly (STB). Figure 1 shows a cutaway view of the FINUDA detector.

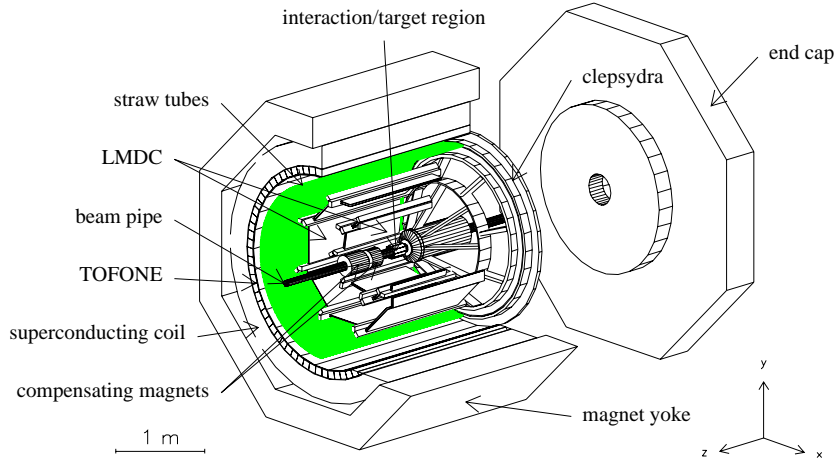


Figure 1: The FINUDA detector.

In order to exploit the large production rate and to measure the π^- momentum as accurately as possible, the detector is designed to have a large geometrical acceptance ($\geq 2\pi$ sr), to be as transparent as possible to minimize momentum degradation and multiple scattering and to have very high spatial resolution and mechanical precision for accurate track reconstruction. The tracking system is optimized to measure π^- coming from the nuclear targets with momenta in the range 250-280 MeV/c with a momentum resolution $\Delta p/p \leq 0.3\%$ FWHM. In order to reach this momentum resolution, a drift chamber spatial resolution of ≤ 150 μm is needed. A more complete description of FINUDA and of its physics program is given in [2–6]. This work presents the results of a cosmic ray test of the low mass drift chambers inside the FINUDA detector without a magnetic field.

2 Experimental Setup

The two main goals of the cosmic ray test were to study the spatial resolution of the final drift chamber modules and their mechanical alignment in the apparatus assembly. For these purposes we used a reduced detector configuration, shown in fig. 2. There was no magnet; the vertex region was replaced by a central

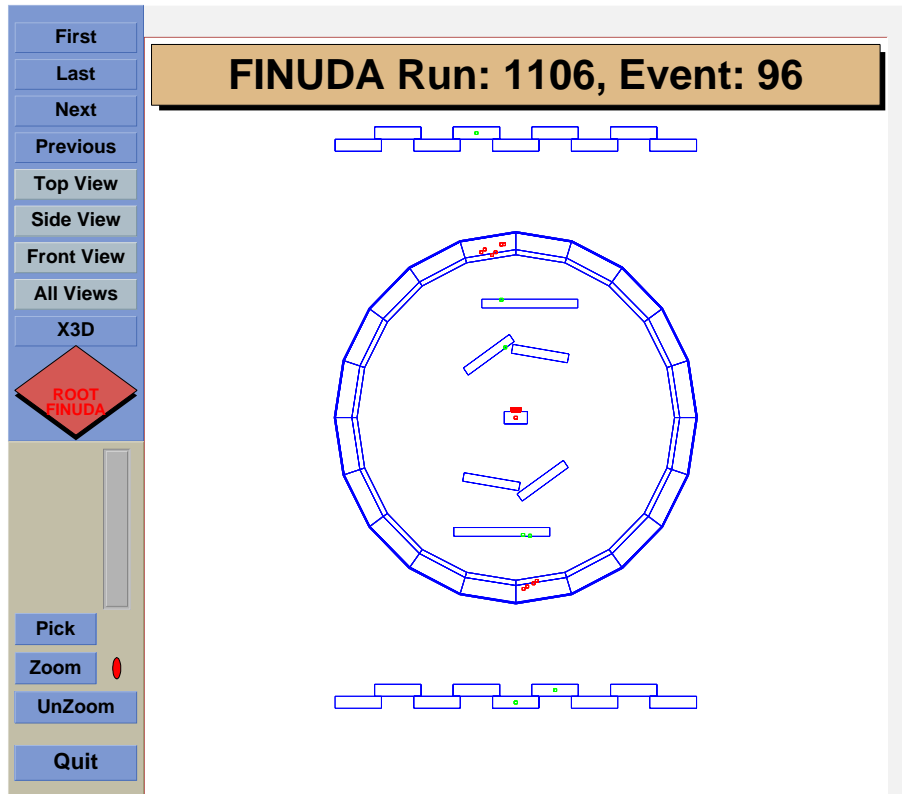


Figure 2: The FINUDA event display graphics in the cosmic ray test layout configuration.

scintillator of dimensions $20 \times 8 \times 3$ cm used for triggering and one microstrip module (SIL); there were only four drift chambers in the inner layer and two in the outer layer, corresponding to the maximum acceptance for cosmic rays passing through the center of the apparatus. The entire straw tube detector was active, but this report presents results concerning only the drift chambers and, in part, the microstrip module; the straw tube data analysis will be presented elsewhere. Finally, there were 18 scintillator slabs (two flat layers of 9 slabs above and below the STB detector) replacing the real Time Of Flight system (TOF).

2.1 Trigger and Data Acquisition

The trigger was realised by means of fast ECL electronics on standard CAMAC and VME modules. It was fully based on the two layers of top and bottom scintillator slabs and on the central slab. All the slabs were viewed by two photomultipliers (PM) at both ends, XP2020 for the central slab and EMI9804B for

the top and bottom layers. After discrimination of the analog signals the hit slabs were defined by Mean Timer circuits (MT), which give a signal with time response independent of the position of the impact point on the slab. The signals coming from MTs of the top and bottom layers were sent to two different ORs. A Programmable Logic Unit (PLU) was used in order to choose two different triggers in the Run Control System menu: a simple coincidence TOP*BOTTOM to select cosmic rays crossing the full apparatus and a coincidence CENTRE*TOP*BOTTOM to select cosmic rays crossing the center of the apparatus and mostly crossing the six drift chambers used and the microstrip module.

The FINUDA final DAQ system [7] was used; it has a tree structure with distributed processes running in parallel on RTPC 8067-LynsOS CPUs, which reside on the Local Event Builders (LEB), one for each detector (TOF, LMDC, STB, SIL). Data read by different LEB are transported via dedicated standard VIC busses to the Global Event Builder (GEB) running also on RTPC. On the contrary the Run Control process runs on an IBM Power PC 601 machine and it communicates with the other processes via socket based network protocols. Data can be written both on disk and on tape. Some events are sampled by the GEB and sent to the monitoring processes through UDP sockets.

The Online Monitor, froot, is based on an object oriented approach in the framework of the ROOT package. It was useful not only to check continuously the detector performances and stability but also to perform a simple pre-analysis of data before using the off-line event reconstruction program. The typical rate with cosmic rays was about 50 Hz with the TOP*BOTTOM trigger and 1.5 Hz with the CENTRE*TOP*BOTTOM trigger. About 730000 central trigger events were recorded.

2.2 Off-line Event Reconstruction

Events passing the trigger requirements are stored in a raw data format and passed to a GEANT-based reconstruction program [2]. The pattern recognition looks for all detector hits geometrically consistent with the passage of a cosmic ray through the apparatus. If at least 3 hits are associated to a cosmic ray, the spatial points are fitted to a straight line. Figure 3 shows a typical cosmic ray event after off-line reconstruction. Although all LMDCs are shown in the off-line event display, we remind the reader that only six chambers were physically present during the cosmic ray test. Off-line reconstruction results are used to study the spatial resolution and alignment of the chambers.

3 The FINUDA Drift Chambers

In this section we give a brief description of the FINUDA drift chambers; for a detailed description see [8–10]. The FINUDA drift chamber design follows the tracking system requirements of large acceptance, transparency and high spatial resolution. The chamber thickness is reduced to a minimum, the mylar windows are very thin (36 μm) and a low mass gas mixture is used. To compensate for the fact that drift velocities in the gas are non-saturated, the electric field inside the drift cells is made as uniform as possible. As shown in fig. 3, in the experimental assembly sixteen planar LMDCs are arranged into two coaxial cylinders of octagonal shape centered on the beam axis. They are rotated one relative to the other by 11° around

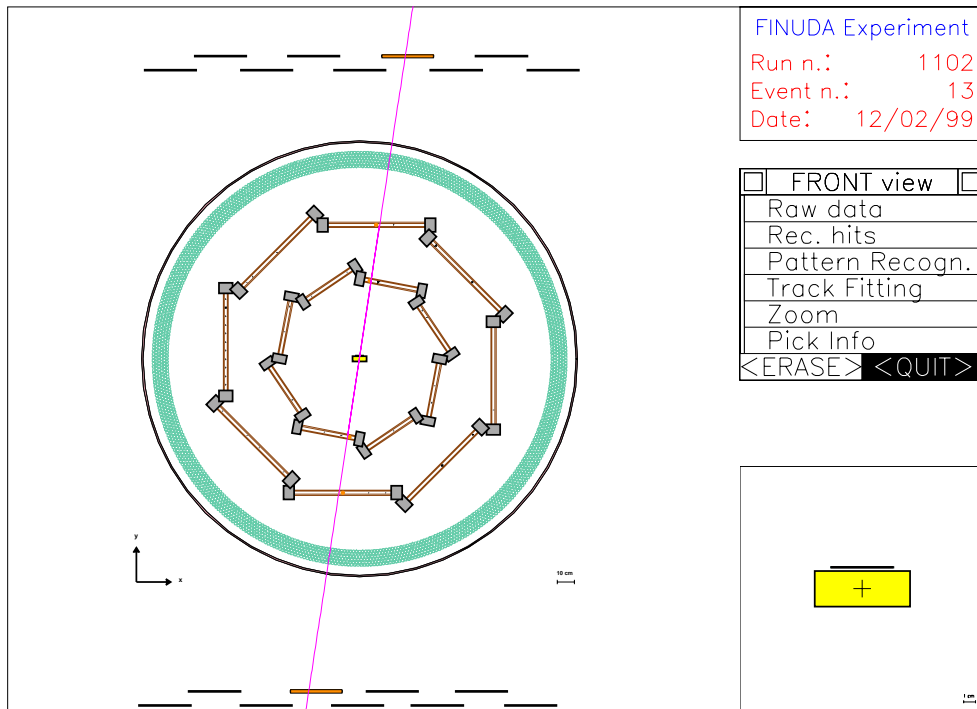


Figure 3: Off-line event display for a typical reconstructed cosmic ray.

their common axis and the lateral sides of the chamber frames overlap in order to maximize acceptance for negatively charged particles of momentum ~ 250 MeV/c. The dimensions of the chambers are 1230 mm \times 396 mm and 1870 mm \times 686 mm for the inner and outer layer, respectively.

3.1 The Drift Cell

The planar LMDCs are made up of contiguous drift cells which operate with a low mass 70% He - 30% iC_4H_{10} mixture. Each cell is 25 mm wide and 6 mm thick. Figure 4 shows the cell layout. There are two parallel layers of cathode wires at a relative distance of 6 mm; the wires are 50 μ m in diameter and are spaced by 1 mm. Wires of the same type were used as field wires in the anode plane, spaced by 50 mm. The left/right ambiguity is solved by using doublets of sense wires: a pair of anode wires spaced by 200 μ m is placed in the center of the cell, and the separation between the anode doublets is 50 mm.

In the presence of a magnetic field, the electron drift lines are tilted. In order to compensate for this *Lorentz* angle, the relative potential distribution between the cathode wire planes is shifted by 1 mm (a shift of one wire) when operating in the FINUDA magnetic field of 1.1 T.

4 Drift Cell Models

The localization accuracy of a drift chamber largely depends on the precise knowledge of the drift space-time relations, which in turn depends on the gas mixture employed and the electric field in the cell. An accurate model of the drift cell is therefore essential for high precision track reconstruction.

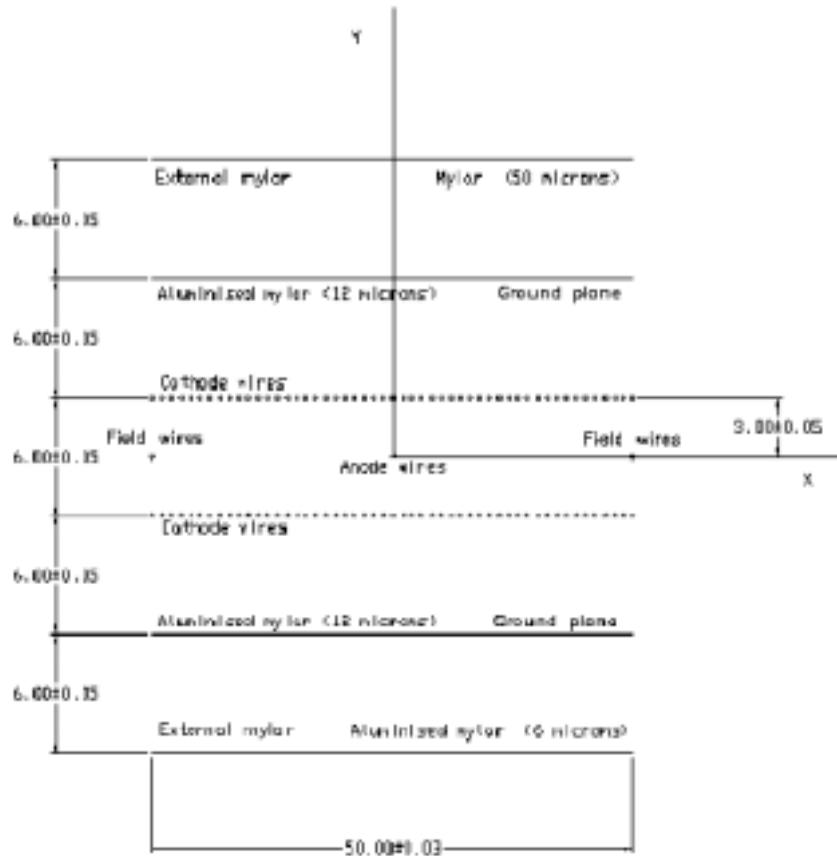


Figure 4: Schematic view of the drift cell structure.

4.1 Constant Velocity Model

As a first approximation, the drift cell can be modeled assuming a constant drift velocity. The mean drift velocity can be inferred from the cell dimensions and the amplitude of the TDC (time) spectra, and it varies slightly from chamber to chamber within the range 33.4 to $33.9 \mu\text{m/ns}$. Figure 5 shows the TDC distribution for a typical cell. Since cosmic rays are randomly distributed, one expects a flat distribution throughout the cell for the crossing point of the cosmic ray on the plane of the sense wires, except for possible inefficiencies close to the anode or to the end walls of the cell. Figure 6a shows such distribution obtained using a constant velocity model. Not surprisingly, the constant drift velocity assumption is too naive for cells using a non-saturated gas, and a more sophisticated model is needed.

4.2 Model using GARFIELD

We study the behavior of the cell using GARFIELD [11], a powerful simulation program for drift chambers. We give as input the cell geometry, the gas mixture, and the field wire voltages. The magnetic field was set

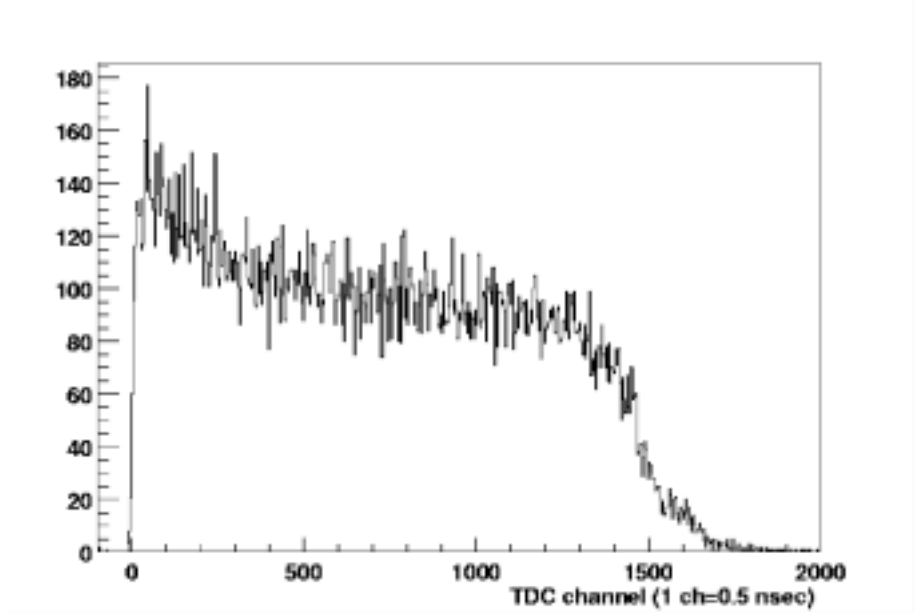


Figure 5: TDC distribution for one cell. The mean drift velocity is estimated from the maximum drift time and the cell dimensions.

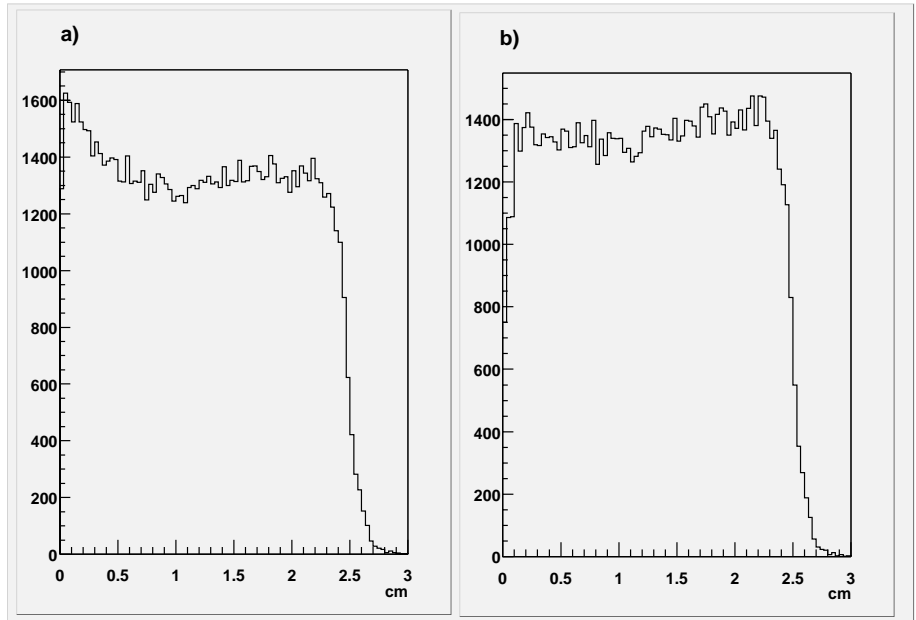


Figure 6: Crossing point of the cosmic ray on the plane of the sense wires. a) constant velocity model, b) cell modeled using GARFIELD.

to zero and therefore the voltages on the cathode wires were not shifted. Figures 7 and 8 show the electron drift lines and the drift space-time relations inside the cell calculated by GARFIELD. Different drift space-

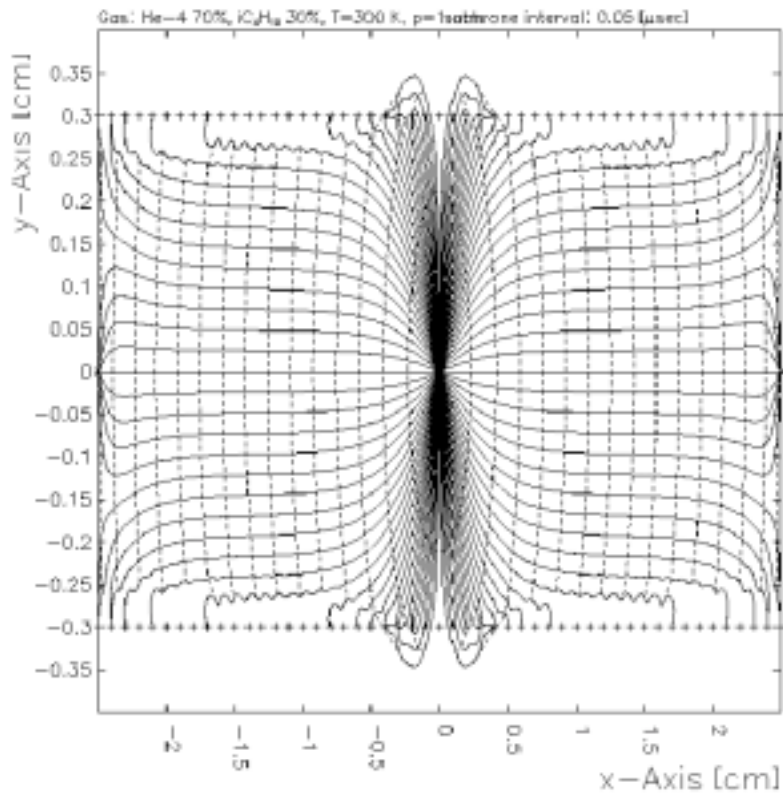


Figure 7: Electron drift lines inside the cell calculated by GARFIELD.

time relation tables are generated for different angles of incidence. In the off-line program, the drift cell structure is reproduced by a linear interpolation between the space-time points calculated by GARFIELD at different angles of incidence. An iterative procedure is then employed where all drift chamber hits are corrected to take into account the angle of incidence (evaluated using the current fit) with respect to the plane of the chamber, until convergence is reached. Figure 9 shows the drift velocity as a function of the distance from the sense wire (on the plane of the sense wire) obtained using GARFIELD, compared to the constant velocity obtained from the TDC spectra. Both models appear to have roughly the same *average* drift velocity and agree reasonably well near the center of the cell; however GARFIELD predicts a completely different behavior near the anode and the end walls.

Figure 6b shows the distribution for the crossing point of the cosmic ray on the plane of the sense wires obtained using the GARFIELD cell model. It is reasonably flat throughout the cell as expected, giving us confidence on the good reproduction of the drift cell by the GARFIELD model.

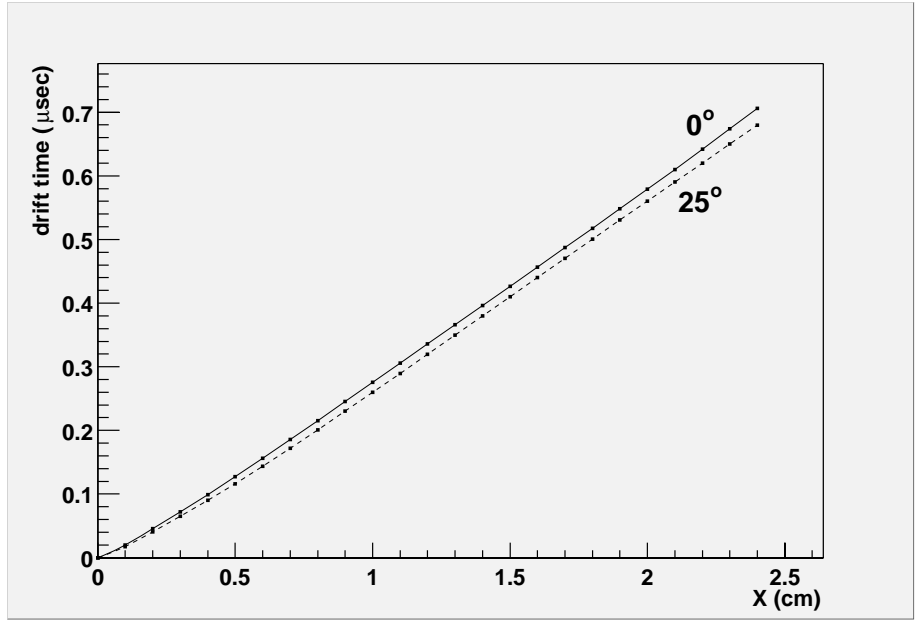


Figure 8: $x(t)$ curves for the cell calculated by GARFIELD for tracks with an angle of incidence of 0° and 25° .

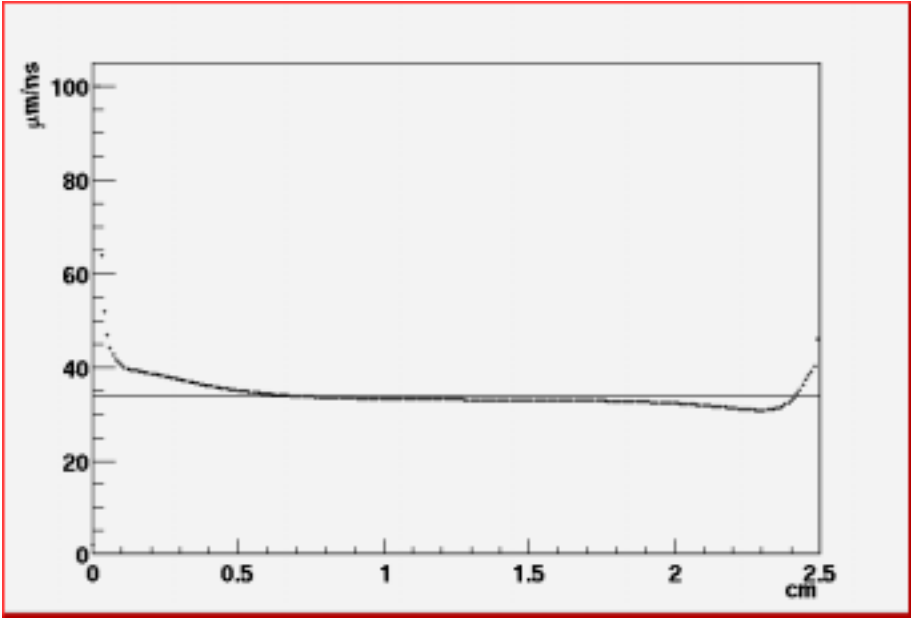


Figure 9: Drift velocity calculated by GARFIELD vs distance from the sense wire on the sense wire plane. The straight line is the constant velocity evaluated from TDC spectra.

5 Data Analysis

Due to effects of finite resolution, misalignment, and multiple scattering, the cosmic ray fit does not pass exactly through the drift chamber hits. The distances between the chamber hits and the points of intersection

of the fit line with the anode planes are called *residuals*, and their study allows us to draw some conclusions about the drift chamber resolution and alignment, as well as to evaluate the effects of multiple scattering due to the presence of the central scintillator slab. We use for the analysis events which have four hits in four different drift cells. Since the measured points are used both for the linear fit and for calculating the residuals, the relation between the drift chamber resolution and the residuals from the fit is given by

$$\sigma_{dch} = \sqrt{N - P} \cdot \sigma_{res} = \sqrt{2} \cdot \sigma_{res}, \quad (1)$$

where $N = 4$ is the number of points used in the fit and $P = 2$ is the number of parameters which determine the straight line, giving two degrees of freedom.

5.1 Resolution and Alignment using the Constant Velocity Model

Even though a constant drift velocity is not the most accurate model for the drift space-time relations, it is nevertheless instructive to use it to study the chamber resolution and alignment. Figure 10 shows the residual distribution for a typical cell using this rough cell model. The width of the distribution gives a resolution of the order of $400 \mu\text{m}$, much larger than the $150 \mu\text{m}$ needed for reaching the design momentum resolution. This resolution, however, is not entirely due to the intrinsic drift chamber resolution, since it has large contributions from effects of multiple scattering, evidenced by the long non-Gaussian tails, and from the fact the the drift cell model used is not very accurate. In the hypothesis that the mechanical

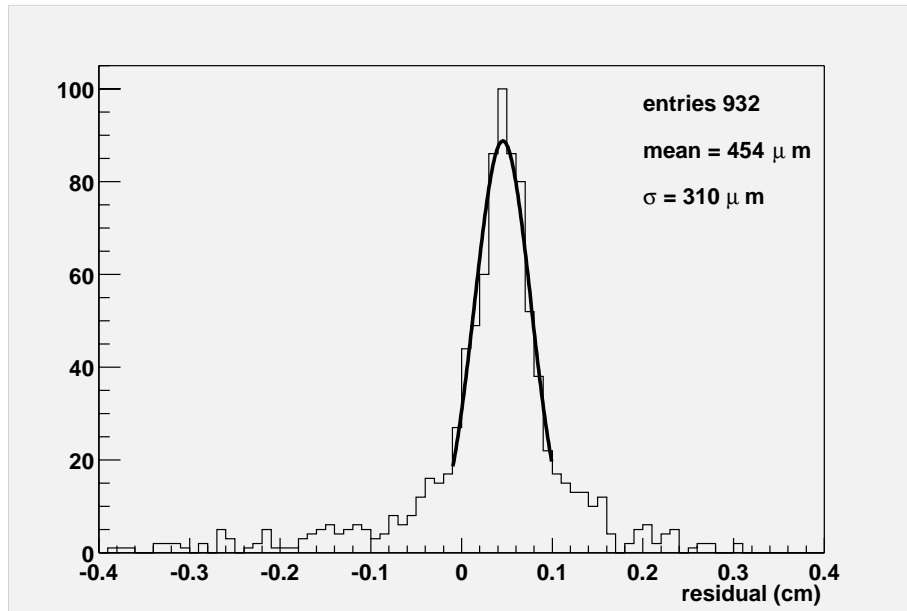


Figure 10: Residuals using the constant velocity drift cell model.

alignment of the drift chambers in the physical detector were exact and that the drift cells were modeled correctly, the residual distributions should have a mean of zero. A displacement of an entire drift chamber

with respect to the others would cause a systematic shift of the means of the residual distributions for all cells. We can therefore control the relative alignment between the chambers by studying the means of the residuals. Figure 11 shows the mean value of the residuals for each wire in one drift chamber. The other chambers show similar patterns. Two problems are evident: the residual distributions for all wires have a

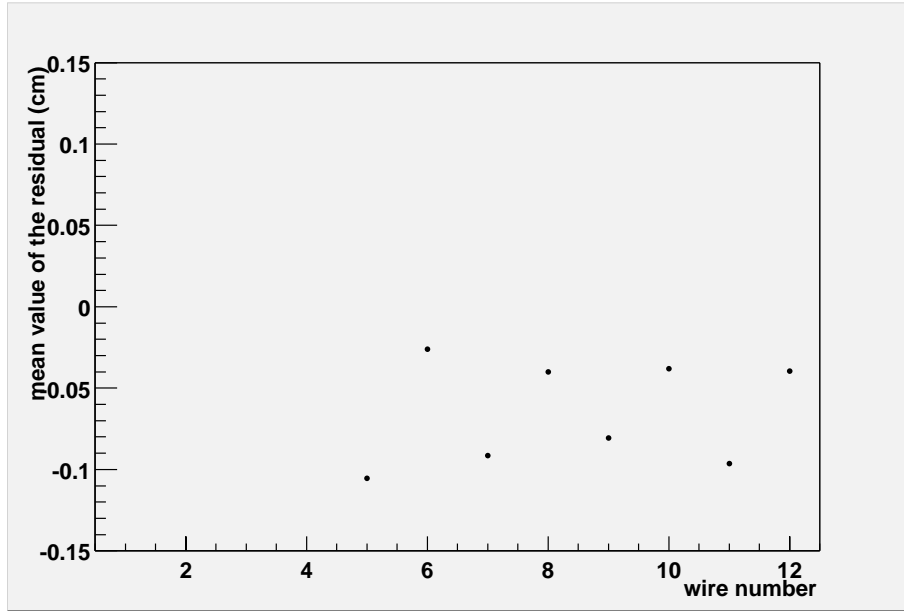


Figure 11: Mean values of the residuals for each wire in a drift chamber obtained using the constant velocity drift cell model.

non-zero mean, and the even and odd numbered wires, or equivalently, the left and right anode wires in each anode doublet are staggered. The first problem results from a misalignment of the drift chamber relative to the other ones. One can “align” this drift chamber by taking the average of all the means and correcting the position of the chamber in the reconstruction software by this amount. This gives a software detector geometry which agrees with that of the physical detector. The second problem is related to the inaccuracy of the constant velocity model, which largely underestimates the drift velocity and, consequently, the electron drift path in the first 5 mm from the wire. A better drift cell model is therefore needed for resolution and alignment studies.

5.2 Resolution and Alignment using GARFIELD

Figure 12 shows the means of the residual distributions for one chamber using GARFIELD to model the drift cell and after the chamber position has been corrected to compensate for the misalignment relative to the other chambers. Because the drift space-time relations are now modeled correctly, there is no more staggering between even and odd numbered wires. The alignment results in mean values around zero as expected. The average geometrical correction needed for the alignment of all chambers studied was less

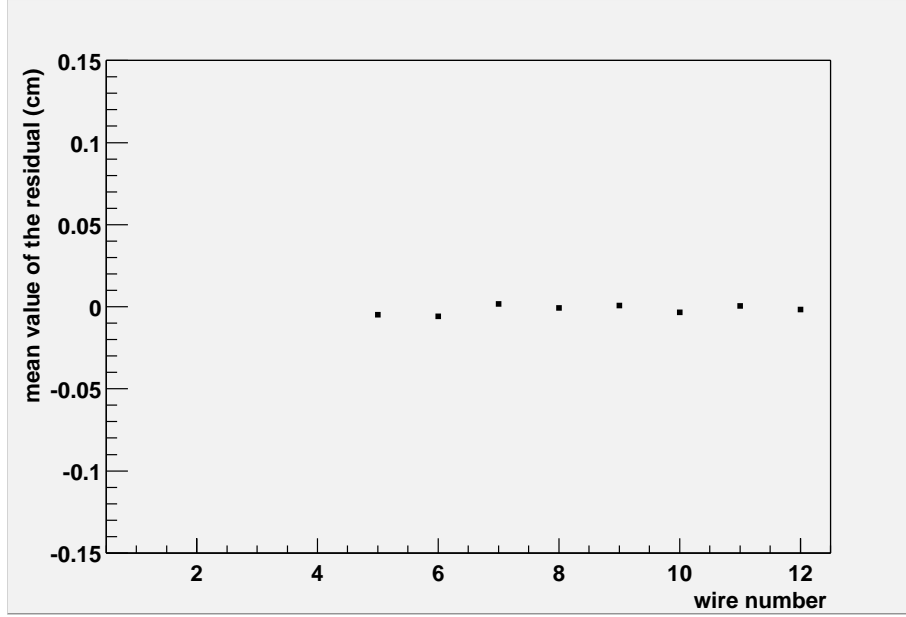


Figure 12: Mean values of the residuals for each wire in a drift chamber obtained using GARFIELD to model the drift cell after the drift chamber has been aligned.

than $350 \mu\text{m}$, which constitutes an excellent performance of the mechanical assembly of the detector. We stress that this is only a relative alignment of the chamber modules and not the absolute alignment in space. For the latter one needs information from independent detectors with high spatial resolution and accuracy (see section 5.4). This alignment does not exclude, however, the possibility of a relative tilt about the longitudinal coordinate z , since the resolutions obtained are averaged over the entire drift chamber length. Higher statistics would allow a determination of the resolutions as a function of the distance from the sense wire and as a function of z , which would yield a more robust alignment. This work will be done for the chambers inside a magnetic field in the final detector configuration. Figure 13 shows the residual distribution for a typical cell obtained using the GARFIELD model. The width of the distribution gives a resolution of the order of $300 \mu\text{m}$, about $100 \mu\text{m}$ better than that obtained using the constant velocity model. This is still larger than the design value due to multiple scattering effects.

5.3 Multiple Scattering Effects

The presence of a central scintillator for triggering causes multiple scattering of the cosmic ray muons, resulting in a widening of the residuals. In order to study the intrinsic drift chamber resolution one needs to separate the contribution due to multiple scattering. A charged particle traversing a scattering medium is deflected on average by an angle [12]

$$\theta = \frac{13.6 \text{ MeV}}{\beta c p} z \sqrt{\frac{x}{X_0}} [1 + 0.038 \ln(\frac{x}{X_0})] \quad (2)$$

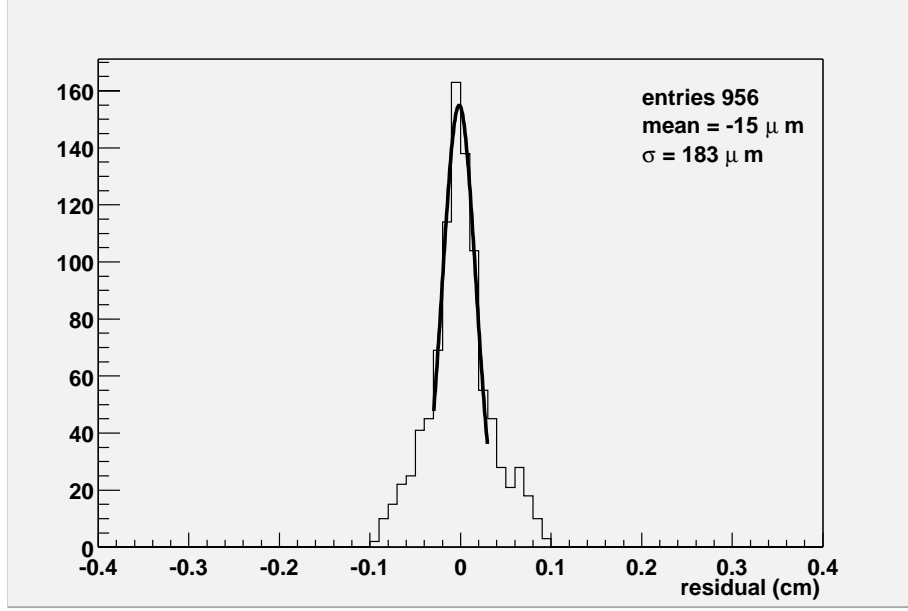


Figure 13: Residuals using the GARFIELD drift space-time relations.

where X_0 and x are respectively the radiation length and the width of the scattering medium, z is the charge of the particle, and p and βc are the momentum and velocity. In our case, for cosmic muons traversing the central scintillator, $z = 1$, $x = 3$ cm, $X_0 = 40$ cm and $p \simeq 2$ GeV/ c , giving an average scattering angle of 1.7 mrad. Figure 14 shows a schematic view of the geometrical setup used to measure the scattering angle caused by the central scintillator, calculated as the angle between the straight line connecting the upper pair of drift chamber hits and the straight line connecting the lower pair of hits. Figure 15 shows the distribution of the scattering angle for cosmic ray muons traversing the central scintillator. The distribution has a width of 2.04 mrad which is due to a convolution of multiple scattering and spatial resolution. In order to separate the effect of multiple scattering we perform a Monte Carlo study with the FINUDA Monte Carlo program [2] based on GEANT [13]. We simulate cosmic ray muons with momentum between 1.5 and 2.5 GeV/ c passing through four drift chambers and the central scintillator. We turn on multiple scattering interactions and assign a constant resolution of $150 \mu\text{m}$ to the drift chambers. Figure 16 shows a comparison between the residuals in the data and those obtained from the Monte Carlo study. Since the data distribution has a smaller width than the Monte Carlo one, we can conclude that the drift chamber resolution contributes less than $150 \mu\text{m}$ to the entire resolution. In fact, using equation 1 one could write

$$\text{data : } 171^2 = \sigma_{ms}^2 + \sigma_{res}^2 \quad (3)$$

$$\text{MC : } 180^2 = \sigma_{ms}^2 + 2 * 150^2 \quad (4)$$

from which $\sigma_{res} = 205 \mu\text{m}$, and $\sigma_{dch} = 140 \mu\text{m}$, within the resolution needed to reach the design momentum resolution.

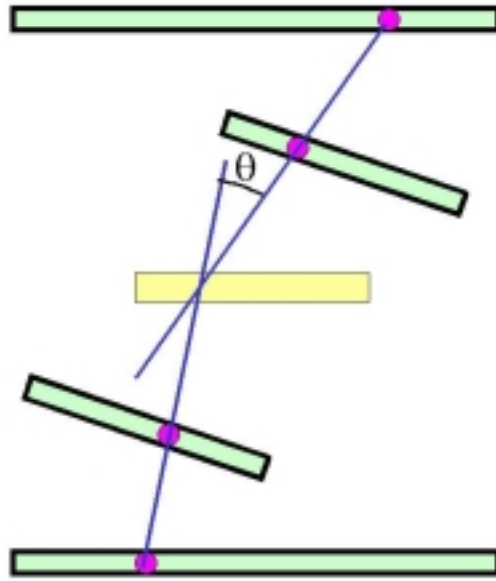


Figure 14: Geometrical setup for the scattering angle measurement.

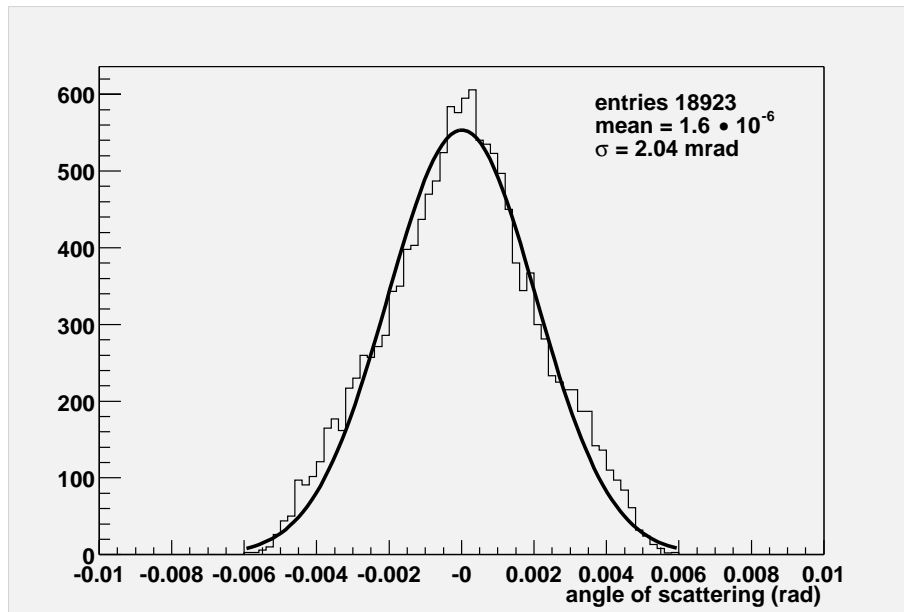


Figure 15: Multiple scattering angle for cosmic ray muons traversing the central scintillator.

5.4 Resolution and Alignment using a Si Microstrip Module

A Silicon microstrip module was placed just above the central scintillator for two main reasons: (i) to obtain an estimate of the *absolute* alignment of the drift chamber assembly with respect to a fixed spatial point and

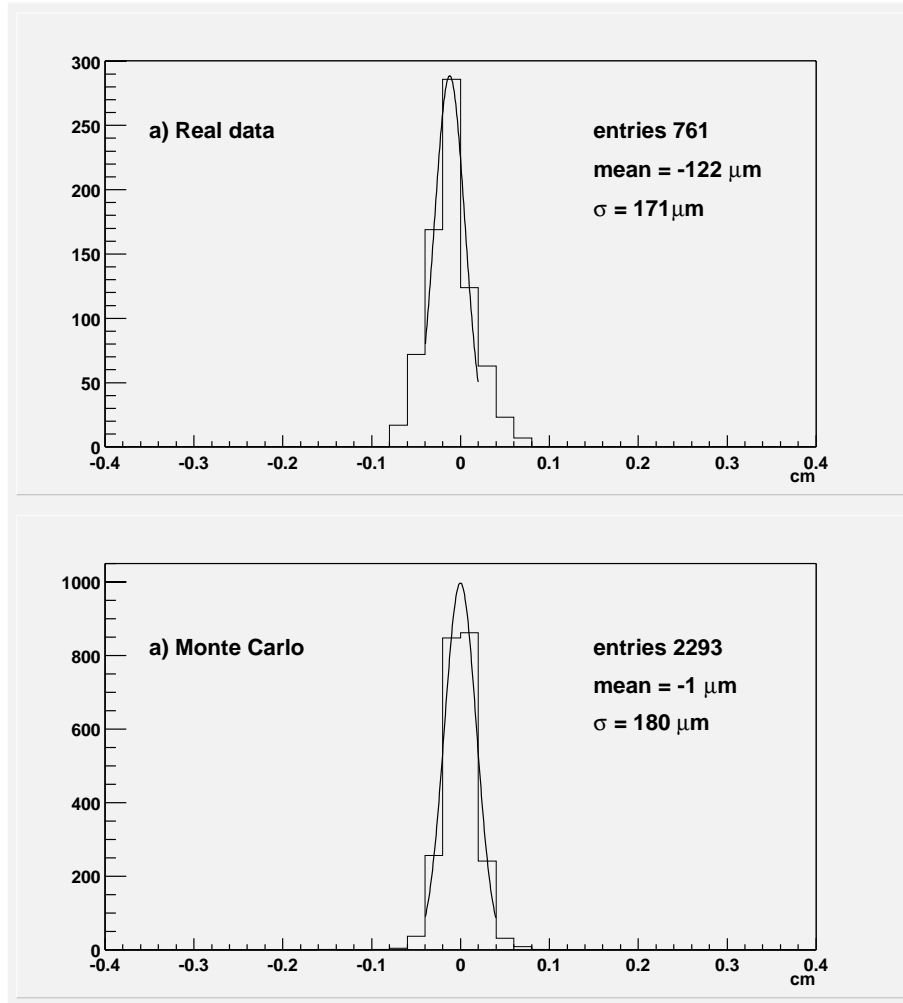


Figure 16: A comparison between the cosmic ray data residuals (a) and Monte Carlo simulation ones (b).

(ii) to obtain a separate determination of the drift chamber resolutions without multiple scattering effects.

Figure 17a shows the distance between the hit on the microstrip module, which is measured with intrinsic resolution of $\sim 20\text{-}30 \mu\text{m}$, and the point of intersection of the fit (using only the four drift chambers) with the plane of the microstrip. The distribution has been centered at zero by displacing the microstrip hits by $440 \mu\text{m}$ during off-line reconstruction. This gives an estimate of the mechanical precision for the alignment and positioning of the microstrip module with respect to the drift chamber system. The width of the distribution ($562 \mu\text{m}$) is the result of the combined effects of multiple scattering and drift chamber resolution. As a check, we performed a Monte Carlo study in which we reproduce the geometrical setup. Again we simulate cosmic ray muons with momentum in the range 1.5 to $2.5 \text{ GeV}/c$ which pass through four drift chambers, the central scintillator, and the microstrip module. We assume a drift chamber resolution of $150 \mu\text{m}$ and turn on multiple scattering interactions. Figure 17b shows the results of the Monte Carlo study:

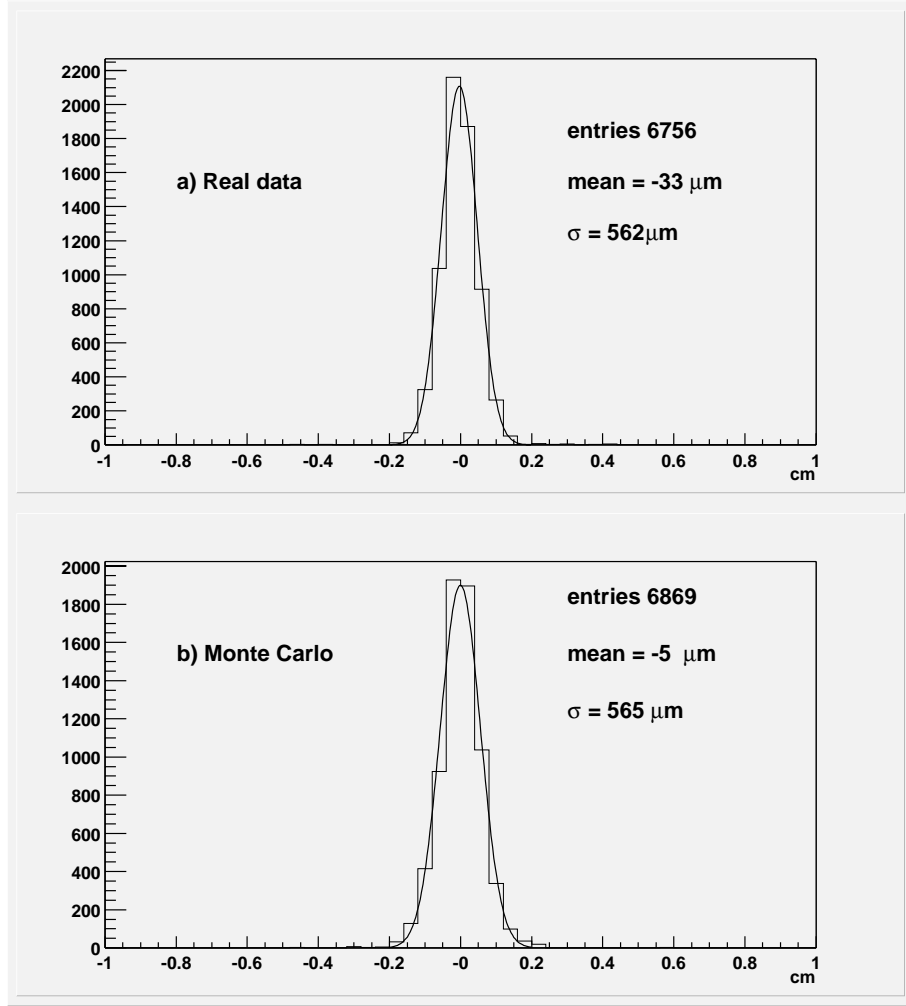


Figure 17: Distance between the hit on the microstrip module and the point of intersection of the fit and the plane of the microstrip for real data (a) and Monte Carlo simulation (b).

the agreement between the Monte Carlo and the data distributions is excellent.

In order to study the drift chamber resolutions avoiding the effects of multiple scattering, we use data from two chambers and the silicon microstrip module located *above* the central scintillator, as illustrated in fig. 18. Figure 19 shows the distance between the measured point in the inner chamber and the line connecting the hits on the microstrip and on the outer chamber. The microstrip resolution is negligible compared to the chamber resolution. The inner chamber is about half way between the outer chamber and the microstrip. If one makes the reasonable assumptions that the microstrip point is fixed and that all drift chambers have similar resolutions, one can therefore write

$$\sigma_d^2 = \sigma_{dch}^2 + \left(\frac{1}{2}\sigma_{dch}\right)^2 = \left(\frac{5}{4}\sigma_{dch}\right)^2. \quad (5)$$

The relation between the width of the distribution ($\sigma_d = 153 \mu\text{m}$) in fig. 19 and the drift chamber resolution

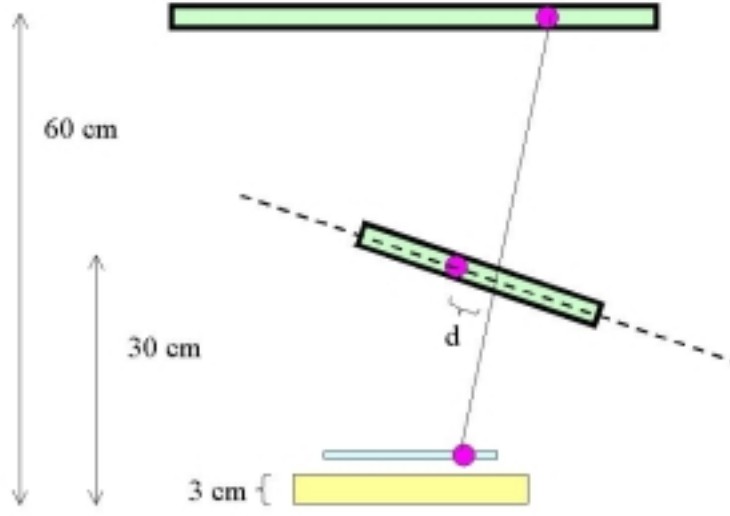


Figure 18: Geometrical setup for the resolution measurement using the microstrip module.

(σ_{dch}) is:

$$\sigma_{dch} = \sqrt{\frac{4}{5}}\sigma_d = 137\mu\text{m}, \quad (6)$$

in excellent agreement with the previous Monte Carlo resolution study.

6 Conclusions

Using cosmic ray data we have measured the FINUDA drift chamber resolution and checked their alignment in the apparatus mechanical structure. We find a resolution of $\sim 140 \mu\text{m}$, within the requirement of $150 \mu\text{m}$ for obtaining the design momentum resolution of the FINUDA spectrometer. All results show excellent agreement with Monte Carlo studies. The resolutions obtained are averaged over all cells, over all angles of incidence, and over all z values. Higher statistics are needed to study the resolutions as a function of the distance from the wires and as a function of the longitudinal coordinate z , and this work will be done in the final detector configuration with the magnetic field. We have shown that the drift chambers can be aligned from a study of the means of the residuals, and that the FINUDA mechanical structure itself yields an excellent alignment of the order of $350 \mu\text{m}$.

References

- [1] M. Agnello et al., Proposal LNF-93/021 (IR) (1993).

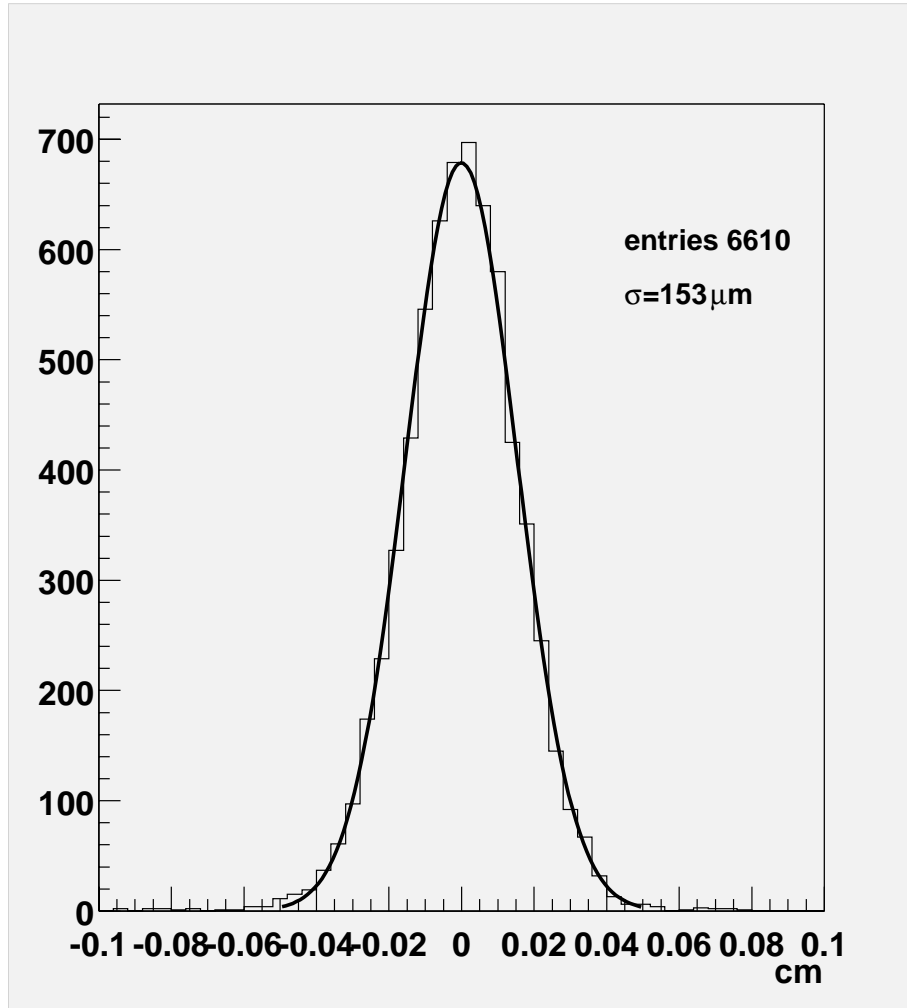


Figure 19: Distance between the measured point in the inner chamber and the line connecting the hits on the microstrip and on the outer chamber.

[2] The FINUDA Collaboration, FINUDA Technical Report, LNF-95/024(IR), (1995).

[3] M. Agnello *et al.*, Nucl. Phys. **A639** (1998) 529c.

[4] M. Agnello *et al.*, Nucl. Phys. **A639** (1998) 537c.

[5] M. Agnello *et al.*, Nuovo Cim. **A111** (1998) 1067.

[6] A. Zenoni for the FINUDA Collaboration, “The physics program of the FINUDA experiment at DAΦNE”, invited talk at *the III Workshop on Physics and Detectors for DAΦNE* (ed. S. Bianco *et al.*, Frascati, Nov. 16-19 1999), Frascati Physics Series **XVI** (1999) 739.

D. Calvo for the FINUDA Collaboration, “The FINUDA Detector”, invited talk at *The III Workshop on*

Physics and Detectors for DAΦNE,(ed. S. Bianco *et al.*, Frascati, Nov. 16-19 1999), Frascati Physics Series **XVI** (1999) 369.

- [7] P. Cerello *et al.*, IEEE Trans. on Nucl. Sci. **45** (4) (1998) 1973.
- [8] M. Agnello *et al.*, Nucl. Instr. Meth. **A367** (1995), 100.
- [9] M. Agnello *et al.*, Nucl. Instr. Meth. **A385** (1997), 58.
- [10] A. Sharma-Gaur, “Study and Optimization of the Tracking Detector for the FINUDA Experiment”, doctoral dissertation thesis, University of Geneva, Geneva (1996).
- [11] GARFIELD R. Veenhof, *GARFIELD, a drift-chamber simulation program*, CERN Program Library entry W5050.
- [12] Particle Data Group, *Review of Particle Physics*, The European Physical Journal **C3**, 1 (1998).
- [13] R. Brun *et al.*, GEANT3, CERN Report DD/EE/84-1 (1987), 1.